C. R. Chimie 17 (2014) 920–926

Contents lists available at ScienceDirect

Comptes Rendus Chimie

www.sciencedirect.com

Full paper/Mémoire

Mechanochemical synthesis and ionic conductivity of lanthanum phosphosilicate oxyapatites

Mécanosynthèse et conductivité ionique d'oxyapatites phosphosilicatées au lanthane

Nadia Gmati [a], Khaled Boughzala [a], Ezzedine Ben Salem [a], Anis Chabene [a], Nabil Fattah [b], Khaled Bouzouita [a,*]

[a] *Institut préparatoire aux études d'ingénieur de Monastir, 5019 Monastir, Tunisia*
[b] *Compagnie des phosphates de Gafsa, Centre de recherche de Metlaoui, 2130 Metlaoui, Tunisia*

ARTICLE INFO

Article history:
Received 22 July 2013
Accepted after revision 28 October 2013
Available online 30 June 2014

Keywords:
Oxyapatite
Rare earths
Mechanochemical method
Ionic conductivity

ABSTRACT

Lanthanum phosphosilicate apatites with the chemical formula $Sr_{10-x}La_x(PO_4)_{6-x}(SiO_4)_xO$, where $0 \leq x \leq 6$, usually prepared by a solid-state reaction at about 1400 °C, were synthesized via the mechanochemical method at room temperature. The samples were characterized using powder X-ray diffraction, infrared spectroscopy and thermal analysis. The results showed that the prepared products were carbonated apatites and no secondary phase was detected. The realization of the milling under a controlled atmosphere can lead to oxyapatites containing no carbonates. The ionic conductivity of the $Sr_6La_4(PO_4)_2(SiO_4)_4O$ sample was investigated by using impedance spectroscopy. The highest ionic conductivity value of 1.522×10^{-6} S·cm^{-1} was found at 800 °C. In the investigated temperature range, the activation energy is of 0.85 eV.

Mots clés :
Oxyapatites
Terres rares
Mécanosynthèse
Conductivité ionique

RÉSUMÉ

Des apatites phosphosilicatées au lanthane de formule chimique $Sr_{10-x}La_x(PO_4)_{6-x}(SiO_4)_xO$ où $0 \leq x \leq 6$, généralement préparées par réaction à l'état solide à environ 1400 °C environ, ont été synthétisées par mécanosynthèse à la température ambiante. Les échantillons ont été caractérisés par diffraction des rayons X, spectroscopie infrarouge et analyse thermique. Les résultats ont montré que les produits obtenus étaient des apatites carbonatées et aucune phase secondaire n'a été détectée. La réalisation du broyage sous atmosphère contrôlée devrait conduire à des oxyapatites ne contenant pas de carbonates. La conductivité ionique de l'échantillon $Sr_6La_4(PO_4)_2(SiO_4)_4O$ a été étudiée par spectroscopie d'impédance. La valeur de la conductivité ionique la plus élevée, $1{,}522 \times 10^{-6}$ S·cm^{-1}, a été déterminée à 800 °C. Dans le domaine de température étudié, l'énergie d'activation est de 0,85 eV.

1. Introduction

Apatites are a large family of compounds with the general chemical formula $M_{10}(XO_4)_6Y_2$, where M represents a divalent cation, XO_4 an anion group and Y a monovalent anion. They crystallize mainly in the

* Corresponding author.
E-mail address: khaled.bouzouita@ipeim.rnu.tn (K. Bouzouita).

1631-0748/$ – see front matter
http://dx.doi.org/10.1016/j.crci.2013.10.018

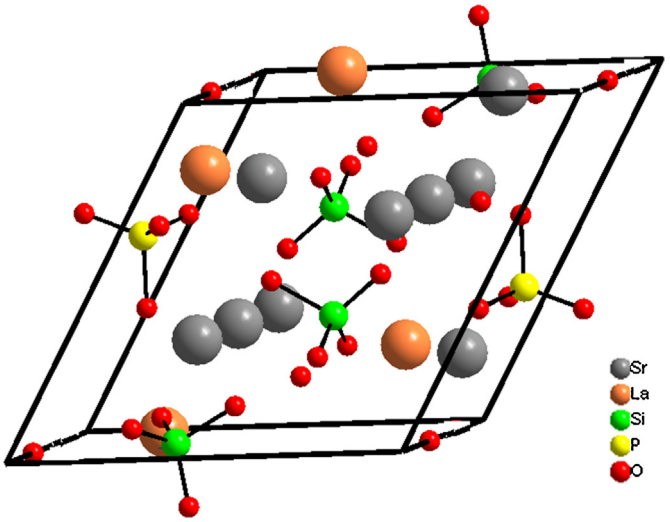

Fig. 1. (Color online). Positions of atoms in the strontium oxyapatite unit cell ($Sr_{10}(PO_4)_6O$).

hexagonal system with the $P6_3/m$ space group [1] (Fig. 1). The main representative member of the apatite family is the hydroxyapatite HA, $Ca_{10}(PO_4)_6(OH)_2$, that can be considered as a wonderful compound. Its chemical composition and crystallographic structure similar to that of the mineral phase of bone and teeth make it a material of choice in many medical applications [2–4]. Furthermore, as a result of its ability to accommodate a great number of substitutions: cationic, anionic or both cationic and anionic substitutions, practically a third of the periodic table elements can be incorporated within the apatite lattice [5,6], making the application field of the obtained materials practically unlimited [7–14]. Indeed, this flexibility of the apatite structure to accept a variety of species may confer to the prepared materials very diverse properties, resulting in a variety of applications that are either already planned or are still to be discovered.

For example, simultaneous substitutions can occur in the three sites (M, XO_4 and Y). In hydroxyapatite, the substitution of La^{3+}, SiO_4^{4-} and $O^{2-}$for Ca^{2+}, PO_4^{3-} and OH^-, respectively leads to new compounds, which have gained considerable interest as oxide ion conductors following the works of Nakayama et al. [15–17]. These compounds are usually prepared by a solid-state reaction at high temperatures. Also, several heat treatments are often required to achieve single-phase materials [18–21]. On the contrary, the mechanochemical synthesis involves only a solid-state reaction at room temperature [22,23]. Therefore, this method appears quite attractive for the preparation of this kind of materials [24,25]. Besides its low energy consumption, simplicity and speed, it is suitable for industrial production. Furthermore, the mechanical treatment leads to an increase in the specific surface area of powders, which should improve the densification of the materials [26].

The aim of this work was to attempt the preparation of the series ($Sr_{10-x}La_x(PO_4)_{6-x}(SiO_4)_xO$, where $0 \leq x \leq 6$) via the mechanochemical method. The obtained powders were investigated using XRD, FTIR and TGA/DTA. In addition, we have characterized the $Sr_6La_4(PO_4)_2(SiO_4)_4O$ sample by its ionic conductivity.

2. Experimental procedure

2.1. Preparation of powders

The samples were prepared by the mecanochemical process using a Retsch PM200 planetary micro mill. The synthesis reaction occurs as follows:

$$4\,SrO + (6\text{-}x)/2\;\; Sr_2P_2O_7 + x/2\;\; La_2O_3 + x\;\; SiO_2 \rightarrow Sr_{10-x}La_x(PO_4)_{6-x}(SiO_4)_xO \quad (1)$$

Appropriate amounts of strontium oxide (SrO), lanthanum oxide (La_2O_3), silica (SiO_2) and strontium diphosphate ($Sr_2P_2O_7$) in order to obtain (Sr + La)/(P + Si) atomic ratios of 1.67 were ground and homogenized in an agate mortar prior to grinding. Then, the mixture was introduced with several stainless steel balls, 10 mm in diameter in a 50 cm^3 stainless steel cell. The weight ratio of the ball-to-powder for all samples was 34:1. The rotating disc speed and cell speed were 500 and 1000 rpm, respectively. Following a previous study [24], the grinding duration was fixed at 25 h. In order to avoid excessive temperature inside the mill cell, milling was carried out in 30 minutes intervals with a 5 minutes pause.

The strontium diphosphate was obtained by heating a mixture of strontium carbonate and di-ammonium hydrogenophosphate at 900 °C for 10 h, while strontium oxide was obtained by calcination of the corresponding carbonate at 1100 °C for 24 h. To avoid deviation from stoichiometry, lanthanum oxide was calcined at 1000 °C for 24 h just before use. Indeed, when La_2O_3 is exposed to air, there is formation of $La_2(OH)_{6-2x}(CO_3)_x$, with $x \approx 1$ [27,28].

In the following sections, the compositions $Sr_{10}(PO_4)_6O$, $Sr_9La(PO_4)_5(SiO_4)O$, $Sr_8La_2(PO_4)_4(SiO_4)_2O$, $Sr_6La_4(PO_4)_2(SiO_4)_4O$, $Sr_5La_5(PO_4)(SiO_4)_5O$ and $Sr_4La_6(SiO_4)_6O$ will be labeled $Sr_{10}O$, Sr_9LaO, Sr_8La_2O, Sr_6La_4O, Sr_5La_5O and Sr_4La_6O, respectively.

2.2. Powder characterization

X-ray diffraction (XRD) patterns of samples were recorded on an X'Pert Pro, PANalytical diffractometer operating with the Cu Kα radiation. The samples were scanned in the 2θ range from 20 to 65° with a step size of 0.01° and a counting time of 1 s per step. The experimental patterns were compared to standards compiled by the Joint Committee on Powder Diffraction and Standards (JCPDS) using the X'Pert HighScore Plus software. The lattice parameters of all samples were determined by the least squared method.

Infrared absorption spectra were recorded in the 400–4000 cm^{-1} range with a PerkinElmer Spectrum 100 spectrometer, using the KBr pellet technique.

Thermal analysis was conducted in air from room temperature to 1000 °C at a heating rate of 10 °C/min, using a Setaram 92 apparatus.

Impedance measurements were carried out on the Sr_6La_4O sample using a Hewlett-Packard 4192-A impedance analyzer, operating at frequencies ranging from 5 to 13 MHz. After milling for 25 h, the powder was pelletized under a pressure of 13 tons. Then, the pellets were heated at 900 °C for 24 h. This temperature was imposed by our furnace capacity. The obtained pellet has a thickness (e) of 0.0885 cm and a surface (S) of 1.252 cm^2. The geometric factor (e/S) of the pellet is 0.07 cm^{-1}. The relative density was of about 60%. Silver electrodes were painted on the two faces of the pellets with a silver paste, and then the painted pellets were heated at 300 °C for 1 h.

3. Results and discussion

3.1. X-ray diffraction

Fig. 2 shows the XRD patterns of samples ground for 25 h. As seen, all the patterns exhibit only the reflections of an apatite phase, indexed in the hexagonal system ($P6_3/m$ space group) based on the strontium oxyapatite, $Sr_{10}(PO_4)_6O$ (JCPDS card No. 00-044-0654), and no evidence of any second phase was found. This indicates that all the prepared samples were single phase. However, the presence of other phosphate compounds as amorphous phase or as impurities in small quantities could not be excluded.

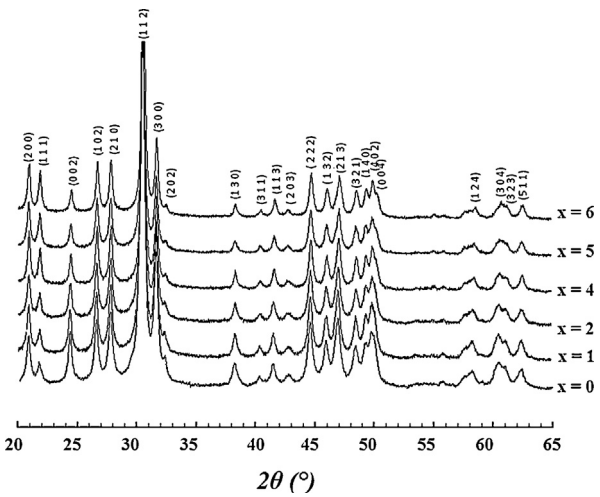

Fig. 2. XRD patterns of all the samples milled for 25 h.

3.2. Infrared spectroscopy

The IR absorption spectra of the samples milled for 25 h are displayed in Fig. 3. The assignments of the different absorption bands were performed according to the literature [29–32]. The similarity of the vibration

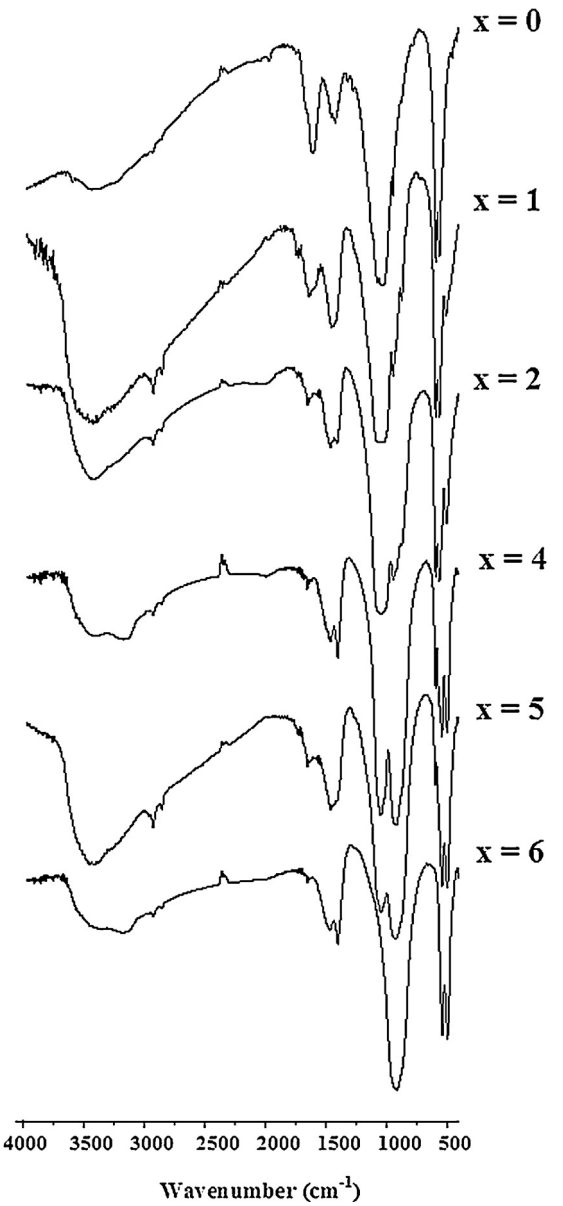

Fig. 3. FTIR spectra of all the samples milled for 25 h.

Table 1
Assignment of the IR absorption bands for the samples milled for 25 h.

Samples	PO_4^{3-}			SiO_4^{4-}		
	ν_1 (cm^{-1})	ν_3 (cm^{-1})	ν_4 (cm^{-1})	ν_1 (cm^{-1})	ν_3 (cm^{-1})	ν_4 (cm^{-1})
$Sr_{10}O$	946	1042 1073	591 561	–	–	–
Sr_9LaO	942	1041	591 563	871	916	504 543
Sr_8La_2O	942	1043	593 564	872	916	505 544
Sr_6La_4O	943	1042	562 595	874	915	499 542
Sr_5La_5O	942	1046	596 –	877	920	498 544
Sr_4La_6O	–	–	–	–	922	540 496

modes of the two tetrahedral groups (PO_4^{3-} and SiO_4^{4-}) has made the identification of the bands somewhat difficult. The assignments of the observed vibrational frequencies of the prepared samples are summarized in Table 1.

For the non-substituted sample, the bands at 1073–1042 and 946 cm^{-1} correspond to P–O stretching vibration modes, while the doublet at 591–561 cm^{-1} corresponds to the O–P–O bending mode. The doublet at 1453 and 1406 cm^{-1}, and the band at about 863 cm^{-1} were assigned to the ν_3 and υ_2 vibration modes of CO_3^{2-} groups. These bands indicate that some PO_4^{3-} groups were partly replaced by CO_3^{2-} ones in the apatite structure (B-type substitution). Therefore, an equivalent amount of SiO_2 was expected to remain in its original form in the powder. It was not detected probably due to its low quantity. The weak band at around 3570 cm^{-1} can be attributed to the stretching mode of the hydroxyl group, indicating that some OH^-groups were inserted into the apatite lattice. Notice the lack of the band at 630 cm^{-1} corresponding to the bending mode of this latter group. Thus, although the grinding was carried out by a dry process, air moisture may result in the incorporation of hydroxyl groups into the apatite structure. It is well known that phospho-oxyapatite is rarely obtained in a pure state [33]. The bands around 3422 cm^{-1}, as well as the band at 1606 cm^{-1}, are related to the adsorbed water on the solid surface. For the substituted samples with $1 \leq x \leq 5$, additional bands appeared at 920, 872 and 500–545 cm^{-1}, they were assigned to the SiO_4^{4-} group. The band located at 920 cm^{-1} is assigned to the asymmetric stretching mode (ν_3) of the Si–O bond, while that at 872 cm^{-1} corresponds to the symmetric stretching mode (ν_1). Finally, the bands between 500 and 545 cm^{-1} are attributed to the asymmetric deformation mode (ν_4). Furthermore, with the increase of the silica amount in the initial mixture, the intensities of the SiO_4^{4-} bands increased, whereas those of the PO_4^{3-} bands decreased. This suggests that the SiO_4^{4-} ions substituted for the PO_4^{3-} ones into the apatite lattice. However, as some carbonate ions were incorporated into the apatite structure, an equivalent amount of SiO_2 would not participate in the reaction. The bands associated with the PO_4^{3-} group disappeared completely for the totally silicated sample ($x = 6$).

3.3. Thermal behavior

TG/DTA curves of the Sr_6La_4O sample milled for 25 h are given in Fig. 4. According to equation (1), the heat treatment must not be accompanied by any weight loss. However, when carbonate groups are incorporated into the apatite structure, in accordance with the charge balance, a certain amount of lanthanum oxide or strontium oxide would not participate in the reaction [24]. It is well known that the lanthanum oxide is very sensitive to moisture and carbon dioxide of air. So, after a prolonged exposure to air, it turns into a mixture of oxide, hydroxide and amorphous hydrated hydroxycarbonate [27,34]. Furthermore, as the FTIR spectroscopic analysis showed that the prepared apatites were carbonated, weight losses should occur during heat treatment. Panteix studying the sintering of $La_{9.33}(SiO_4)_6O_2$ observed that although the pellets are sufficiently densified, they degraded when they are left long enough in the air. He attributed this phenomenon to the very high hydrophilicity of the unreacted La_2O_3 and to its sensitivity to air carbon dioxide [27].

The TG profile (Fig. 4) indicated that the weight loss occurred in three temperature ranges. The first weight loss of 0.9% observed in the range from 280 to 350 °C is due to the dehydration of $La(OH)_3$ and $La_2(OH)_4CO_3{\cdot}nH_2O$ to LaOOH and $La_2O_2CO_3$, respectively. The second weight loss of 0.4% achieved at 480 °C was attributed to the departure of water resulting from the transformation of LaOOH into La_2O_3 [27,28,34]. These dehydrations are related to the two first endothermic peaks positioned on the DTA curve at 326 and 473 °C, respectively. The third weight loss of 5.6% occurring between 640 and 900 °C is related to the decarbonation of $La_2O_2CO_3$ [27,34] and the apatite, The departure of CO_2 is illustrated on the DTA curve by the third and the fourth effects at 737 and 870 °C. It is worth noting that no traces of unreacted oxides or carbonates were detected on the XRD patterns, due probably to their amounts that were below the detection limit of XRD.

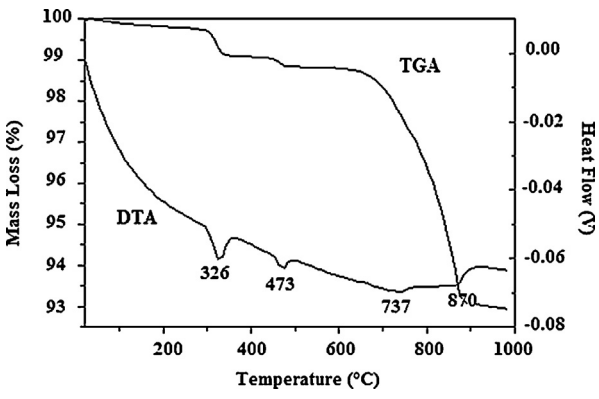

Fig. 4. Thermal analysis of the sample Sr_6La_4O milled for 25 h.

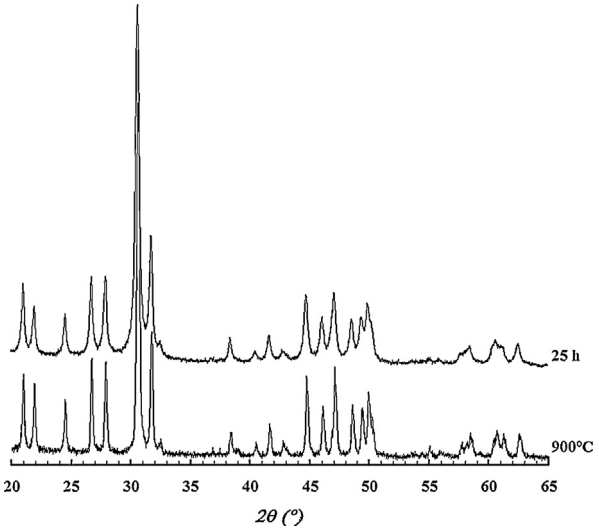

Fig. 5. XRD patterns of the sample Sr_6La_4O milled and calcined at 900 °C.

The XRD pattern of Sr_6La_4O sample milled for 25 h and calcined at 900 °C for 24 h shows that the powder was formed by a pure apatite phase, and no secondary phases were detected (Fig. 5). As observed in Fig. 6, the heat treatment did not cause any significant change in the IR spectrum. It indicates only a decrease in the intensity of bands associated with the carbonate ions.

3.4. Lattice parameters

The lattice parameters are given in Table 2. For the non-substituted sample, the values of $a = 9.749(2)$ Å and $c = 7.270(3)$ Å are lower than those reported in the JCPDS card No. 00-044-0654 ($a = 9.7670$ Å and $c = 7.2890$ Å). With the substitution, the a parameter increased, while c decreased. The changes in the lattice parameters confirm once again that the pair (La^{3+}, SiO_4^{4-}) has entered the apatite structure [24]. However, the interpretation of the variation of the parameters with substitution remains difficult because of the difference in size of the substituent ions (Table 3) [35]. Furthermore, after the insertion of some carbonate ions into the apatite lattice, as it was indicated by IR absorption spectroscopy, the interpretation becomes more complicated. However, it is possible to draw some conclusions. In the apatite lattice, the a-axis is rather influenced by the size of the M(2) site, the anionic tetrahedron and the anion of the tunnel, while the c-axis is mainly influenced by the size of the M(1) site. In the present study, the PO_4^{3-} group (the average length of P–O is 1.51 Å) is replaced by both a more and a less voluminous groups, SiO_4^{4-} (the average length of Si-O is 1.62 Å) and CO_3^{2-} (the average length of C–O is 1.25 Å) [35]. In addition, Sr^{2+} ($^{VII}r_{Sr^{2+}} = 1.21$ Å; $^{IX}r_{Sr^{2+}} = 1.31$ Å) was substituted by a less voluminous ion La^{3+} ($^{VII}r_{La^{3+}} = 1.10$ Å; $^{IX}r_{La^{3+}} = 1.216$ Å) [35].

As was shown in ref. [24], following these substitutions, there was creation of vacancies in the cationic sites. In the apatite structure, the cations are distributed between two nonequivalent crystallographic sites. Four cations per unit cell occupying the (4f) sites are arranged along the three-fold axis. The six other cations located in the (6 h) sites are positioned in the summit of two alternated equilateral triangles, centered on a helical six-fold axis of the structure. The alignment in columns, and the shorter distances between the (4f) sites cause strong repulsions between the La^{3+} ions located in these sites, while the higher distances between the (6 h) sites make them more suitable to minimize the repulsions. Therefore, these latter sites should be fully occupied by the cations and the vacancies should be present only at the (4f) sites. This assumption is supported by the Rietveld refinement of $La_{9.33}(SiO_4)_6O_2$, which showed that all of the vacancies are present at the (4f) sites [36]. Vacancies were also created in

Table 2
Lattice parameters for the samples milled for 25 h.

Samples	a (Å)	c (Å)	V(Å^3)
$Sr_{10}O$	9.749 (2)	7.270 (3)	599.06 (3)
Sr_9LaO	9.752 (1)	7.269 (3)	599.35 (1)
Sr_8La_2O	9.756 (3)	7.265 (2)	599.51 (3)
Sr_6La_4O	9.758 (2)	7.263 (2)	599.59 (2)
Sr_5La_5O	9.762 (3)	7.260 (4)	599.83 (3)
Sr_4La_6O	9.767 (4)	7.258 (2)	600.28 (2)

Table 3
The ionic radii of the different ions.

	Sr^{2+}	La^{3+}	P^{5+}	Si^{4+}	C^{4+}
	CN7/CN9	CN7/CN9	CN4	CN4	CN4
Ionic radii (Å)	1.21/1.31	1.10/1.22	0.17	0.26	0.15

CN: coordinence number.

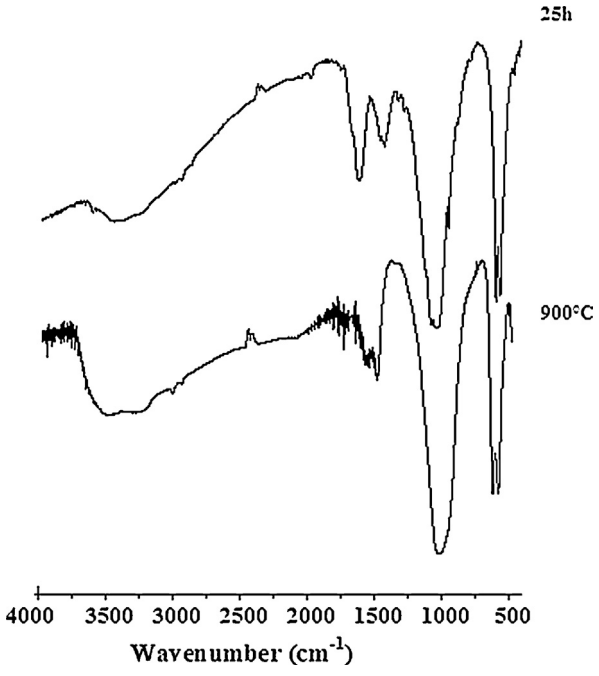

Fig. 6. FTIR spectra of the sample Sr_6La_4O milled and calcined at 900 °C.

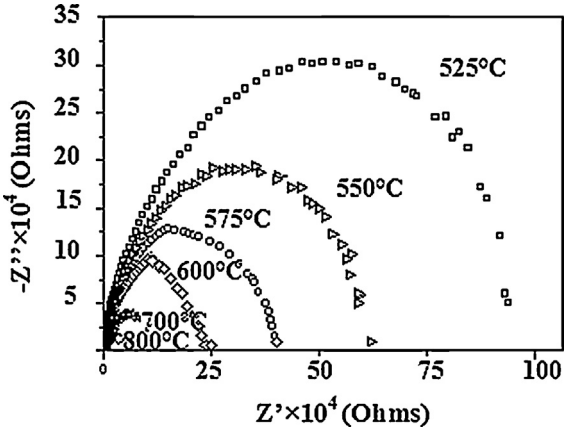

Fig. 7. The impedance plots of Sr_6La_4O at different temperatures.

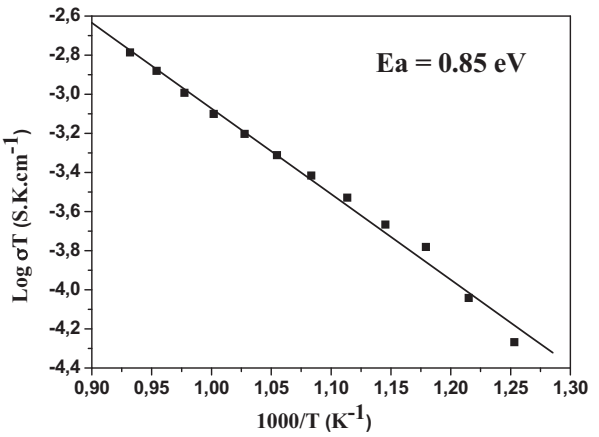

Fig. 8. Plot of log σT (S·K·cm^{-1}) versus 1000/T (K^{-1}) for Sr_6La_4O.

the anionic tunnel following the substitution of $O^{2-}$for OH^-. Thus, it appears that the contraction of the *c* parameter is due to the replacement of Sr^{2+} by a smaller ion, La^{3+}, on the one hand, and to the presence of vacancies along this axis, on the other hand, while the increase of the *a* parameter is due to the contraction following the *c*-axis. The explanation of the effect of substitution on the *a*-axis is not as obvious because of the different sizes of the substituted ions. The comparison of the obtained parameter values with those determined by K. Boughzala for the same compounds, prepared at high temperature [37], shows the same trend as a function of *x* for the two parameters. It is worth noting that these compounds are free of carbonates. Our values are weaker probably because of the incorporation of carbonates into the apatite structure (see § 3.2.).

3.5. Ionic conductivity

Typical complex impedance plots of the Sr_6La_4O sample taken in the 525–800 °C range are illustrated in Fig. 7. As seen, the impedance response of the sample consists of semicircular arcs. The value of resistance at different temperatures has been obtained from the intercept of the semicircular arcs on the real axis, and the electrical conductivity at different temperatures was calculated using the following equation: $\sigma = e/R{\cdot}s$, where R is the resistance determined from impedance plots, and e and s are the thickness and the area of the sample, respectively. The obtained values increased with increasing temperature, varying from 6.76×10^{-8} to 1.52×10^{-6} S·cm^{-1} for 525 and 800 °C, respectively, indicating a thermally activated conduction mechanism. These values correspond to the total conductivity because of the difficulty to separate the grain and bulk boundary contribution from the diagrams.

The temperature dependence of the ionic conductivity has been analyzed using an Arrhenius equation: $\sigma\ T = A\ \exp(-E_a/kT)$, where σ, A, E_a, k and T are the conductivity, pre-exponential factor, activation energy, Boltzmann constant and absolute temperature, respectively. Fig. 8 shows the Arrhenius plot of the sample. The activation energy E_a, determined from the slope of the previous plot, is 0.85 eV.

It is well known that for the rare earth silicate oxypatites, the highest conductivity is observed for the samples containing cationic vacancies and/or an oxygen excess [38,39]. Compared to the lanthanum silicate oxyapatite ($La_{9.33}(SiO_4)_6O_2$) [40], the studied material has a lower conductivity. This can be explained, on the one hand, by the high porosity of the material (relative density = 60%) and on the other hand, by its structure features. As was revealed by IR spectroscopy analysis, all carbonates have not been completely eliminated after heat treatment at 900 °C. Therefore, with respect to the oxyapatite-type $La_{9.33}SiO_{26}$, the carbonate ions, and those of phosphate contracted the *a*-axis, in accordance with their respective sizes. It results a contraction of the tunnel containing oxide ions, limiting therefore the movement of these latter ions. Indeed, it was shown that a high conductivity is characterized by larger channels, in addition to the cationic vacancies [41]. Panteix et al. studying the influence of anionic vacancies on the ionic conductivity of the lanthanum silicate oxyapatite observed that the conductivity is enhanced and the activation energy is decreased for the low levels of oxygen vacancies, while for the high levels, the conductivity is lower and the activation energy is higher [42]. Therefore, the anionic vacancies due to the substitution of $O^{2-}$by OH^-contributed to lowering the conductivity for our sample. In contrast to the fully stoichiometric sample, $Sr_6La_4(PO_4)_4(SiO_4)_2O_2$ [40], the compound investigated in the present work had a higher conductivity, confirming once again that this latter contained cationic vacancies, obviously in addition to the anionic vacancies.

4. Conclusion

Oxyapatites with the chemical formula $Sr_{10-x}La_x(PO_4)_{6-x}(SiO_4)_xO$ (where $0 \leq x \leq 6$) have been prepared from SrO, $Sr_2P_2O_7$, La_2O_3 and SiO_2 using the mechanochemical process. The obtained powders have been characterized by X-ray diffraction, infrared spectroscopy, and thermogravimetric and differential thermal analysis. The results indicated that

the powders were single phase. However, they were carbonated, due to the air carbon dioxide. The electrical properties of the $Sr_6La_4(PO_4)_2(SiO_4)_4O$ sample was investigated by using complex impedance analysis. The highest ionic conductivity of 1.52×10^{-6} S·cm^{-1} was obtained at 800 °C and the ionic jump activation energy is of 0.85 eV.

References

[1] S. Náray-Szabó, J. Z. Kristallogr. 75 (1930) 387.
[2] M. Jarcho, J. Clin. Ortho. Rel. Res. 157 (1981) 259.
[3] L.L. Hench, J. Wilson, Advanced Series in Ceramics, vol. 1, Word Scientific, USA, 1998.
[4] R.Z. Legeros, in: H.M. Myers (Ed.), Monographs in Oral Science, vol. 15, Karger, New York, 1991.
[5] J.C. Elliott, Structure and Chemistry of the Apatites and Other Calcium Orthophosphates, Elsevier, Amsterdam, 1994.
[6] N. Leroy, E. Bres, J. Eur. Cel. Mater. 2 (2001) 36.
[7] M. Sivakumar, K. Panduranga Rao, J. Biomed. Mater. Res. 65A (2003) 222.
[8] J.P. Budin, J.C. Michel, F. Auzel, J. Appl. Phys. 50 (1979) 641.
[9] L.D. Deloach, S.A. Payne, L.K. Smith, W.L. Kway, W.F. Krupke, J. Opt. Soc. Am. B (1994) 269.
[10] K. Gallagher, J. Earth Planet. Sci. Lett. 136 (1995) 421.
[11] K.H. Butler, Fluorescent Lamp Phosphors, University Press, 1986.
[12] N. Dacheux, N. Clavier, A. Robisson, O. Terra, F. Audubert, J. Lartigue, C. Guy, C. R. Chimie 7 (2004) 1141.
[13] E. Du Fou de Kerdaniel, N. Clavier, N. Dacheux, O. Terra, R. Podor, J. Nucl. Mater. 362 (2007) 451.
[14] Q.Y. Ma, S.J. Traina, T.J. Logan, J.A. Ryan, J. Environ. Sci. Technol. (1993) 1803.
[15] S. Nakayama, H. Aono, Y. Sadaoka, J. Chem. Lett. (1995) 431.
[16] S. Nakayama, M. Sakamoto, J. Eur. Ceram. Soc. 18 (1998) 1413.
[17] S. Nakayama, M. Sakamoto, M. Higuchi, K. Kodaira, M. Sato, S. Kakita, T. Suzuki, K. Itoh, J. Eur. Ceram. Sco. 19 (1999) 507.
[18] L. Boyer, J. Carpena, J.-L. Lacout, Solid State Ionics 95 (1997) 121.
[19] K. Boughzala, E. Ben Salem, A. Ben Chrifa, E. Gaudin, K. Bouzouita, J. Mater. Res. Bull. 42 (2007) 1221.
[20] O. Terra, N. Dacheux, F. Audubert, R. Podor, J. Nucl. Mater. 352 (2006) 224.
[21] O. Terra, F. Audubert, N. Dacheux, C. Guy, R. Podor, J. Nucl. Mater. 366 (2007) 70.
[22] A.E. Yermakov, E.E. Yurchikov, V.A. Barinov, J. Phys. Met. Metallogr. 52 (1981) 50.
[23] C.C. Koch, O.B. Cavin, C.G. Mekamey, J.O. Scarbrough, J. Appl. Phys. Lett. 43 (11) (1983) 1017.
[24] N. Gmati, K. Boughzala, M. Abdellaoui, K. Bouzouita, C. R. Chimie 14 (2011) 896.
[25] N. Gmati, K. Boughzala, A. Chaabène, N. Fattah, K. Bouzouita, C. R. Chimie 16 (2013) 712.
[26] J. Meng, C.C. Jia, Q. He, Powder Metall. 51 (2008) 227.
[27] P.J. Panteix, I. Julien, D. Bernache-Assollant, P. Abelard, J. Mater. Chem. Phys. 95 (2006) 313.
[28] T. Kharlamova, S. Pavlova, V. Sadykov, O. Lapina, D. Khabibulin, T. Krieger, V. Zaikovskii, A. Ishchenko, A. Salanov, V. Muzykantov, N. Mezentseva, M. Chaikina, N. Uvarov, J. Frade, C. Argirusis, Solid State Ionics 179 (2008) 1018.
[29] B.O. Fowler, J. Inorg. Chem. 13 (1974) 194.
[30] S. Khorari, R. Cahay, A. Rulmont, Eur. J. Solid State Inorg. Chem. 31 (1994) 921.
[31] J. Neubauer, H. Pollmann, Neues Jahrb. Mineral. Abd 168 (1995) 58.
[32] O. Terra, F. Audubert, N. Dacheux, C. Guy, R. Podor, J. Nucl. Mater. 354 (2006) 49.
[33] K. Ardhaoui, J. Rogez, A. Ben cherifa, M. Jemal, M. Jemal, P. Satre, J. Therm. Anal. Cal. 86 (2) (2006) 553.
[34] E. Béchade, I. Julien, T. Iwata, O. Masson, P. Thomas, E. Champion, K. Fukuda, J. Eur. Ceram. Soc. 28 (2008) 2717.
[35] R.D. Shannon, J. Acta Crystallogr. A 32 (1976) 751.
[36] Y. Masubuchi, M. Higuchi, T. Takeda, S. Kikkawa, J. Solid State Ionics 177 (2006) 263.
[37] K. Boughzala, S. Nasr, E. Ben Salem, F. Kooli, K. Bouzouita, J. Chem. Sci. 121 (3) (2009) 283.
[38] E. Kendrick, M.S. Islam, P. Slater, J. Mater. Chem. 17 (2007) 3104.
[39] W. Liu, S. Yamaguchi, T. Tsuchiya, S. Miyoshi, K. Kobayashi, W. Pan, J. Power Sources 235 (2013) 62.
[40] A. Najib, J.E.H. Sansom, P.R. Slater, M.S. Islam, J. Dalton Trans. (2004) 3106.
[41] S. Guillot, S. Beaudet-Savignat, S. Lambert, P. Roussel, R.N. Vannier, Solid State Ionics 185 (2011) 18.
[42] P.-J. Panteix, E. Béchade, I. Julien, P. Abélard, D. Bernache-Assollant, J. Mater. Res. Bull. 43 (2008) 1223.